Journal of Thermal Analysis Vol. 46 (1996) 1113-1132

Dedicated to Professor Bernhard Wunderlich on the occasion of his 65th birthday

ANALYSIS OF A SYMMETRIC NEOPOLYOL ESTER II. Solid state ^{13}C NMR and X-ray measurements

W. Chen[1,2], *A. Habenschuss*[2], *M. Pyda*[1,2], *Manika Varma-Nair*[3], *H. S. Aldrich*[3] *and B. Wunderlich*[1,2]

[1]Department of Chemistry, University of Tennessee, Knoxville, TN 37996-1600
[2]Chemistry and Analytical Sciences Division, Oak Ridge National Laboratory, Oak Ridge, TN 37831-6197
[3]Corporate Research, Exxon Research and Engineering Company, Linden, NJ 07036, USA

Abstract

The symmetric neopolyol ester tetra[methyleneoxycarbonyl(2,4,4-trimethyl)pentyl]methane (MOCPM) has been studied by variable-temperature solid-state ^{13}C NMR and X-ray powder diffraction and compared to molecular mechanics calculations of the molecular structure. Between melting and glass transition temperatures the material is semicrystalline, consisting of two conformationally and motionally distinguishable phases. The more mobile phase is liquid-like and is, thus attributed to an amorphous phase (≈16%). The branches of the molecules in the crystal exhibit two conformationally distinguishable behaviors. In one, the branches are well ordered (≈56%), in the other, the branches are conformationally disordered (≈28%). Different branches of the same molecule may show different conformational order. This unique character of the rigid phase is the reason for the deficit of the entropy of fusion observed earlier by DSC. In the melt, solid state NMR can identify two bonds that are rotationally immobile, even though the molecules as a whole have liquid-like mobility. This partial rigidity of the branches accounts quantitatively for the observed increase in heat capacity at the glass transition. The reason for this unique behavior of MOCPM, a small molecule, is the existence of one chiral centers in each of the four arms of the molecule. A statistical model assuming that at least two of the chiral centers must fit into the order of the crystal can explain the crystallization behavior and would require 12.5% amorphous phase, 28.1% conformational disorder, and 59.4% crystallinity, close to the observed maximum perfection.

Keywords: chiral molecule, conformational disorder and motion, crystal, DSC, heat capacity, *γ-gauche* effect, glass, glass transition, melting transition, molecular mechanics computations, tetra[methyleneoxycarbonyl (2,4,4-trimethyl) pentyl] methane, solid state ^{13}C NMR, X-ray diffraction

Introduction

The molecular structure of a symmetric neopentane ester tetra[methyleneoxycarbonyl(2,4,4-trimethyl)pentyl]methane is shown below with the number-

0368–4466/96/ $ 5.00

John Wiley & Sons, Limited
Chichester

ing of the distinguishable carbon atoms used in this research. The name of this molecule is abbreviated to MOCPM, following the suggestion in Ref. [1].

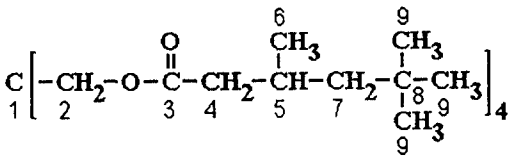

The rather bulky structure of the molecule is shown in Fig. 1 in a conformation that approaches minimal steric hindrance. The figure shows a structure that must be rather difficult to pack closely in a crystal, particularly because carbon atom 5 represents a chiral center. Since no sterically specific synthesis method was used, one expects that the two possible isomers are randomly distributed over the four arms of the molecule. This stereo irregularity and the bulkiness of the molecule are at the root of the difficult crystallization and the unique solid phase structure and mobility.

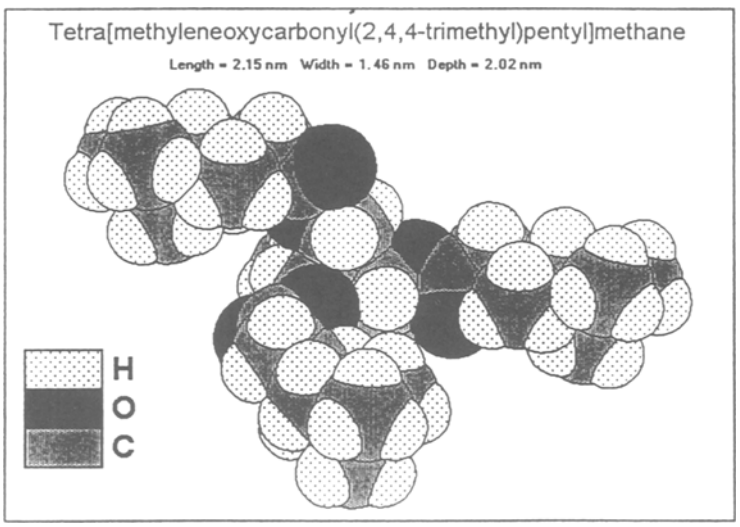

Fig. 1 Molecule of MOCPM in a low energy conformation. The fourth branch of the molecule is pointing towards the back

Samples of MOCPM have been studied by differential scanning calorimetry (DSC) [1] with the result that they can be produced as samples of high, but incomplete, crystallinity (70–90%) or quenched to a glass. The amorphous MOCPM has a glass transition temperature of 219 K, the semicrystalline, a melting temperature of 304 K. Although the melting may show a second endotherm at somewhat lower temperature, this can be annealed to the 304 K melting peak, i.e. there seems to be no stable mesophase between the glass and melting transition. For a fully amorphous sample the change in heat capacity at

the glass transition is 250 J K^{-1} mol^{-1}. This change in heat capacity can be attributed to an approximate number of 22 "beads" in the molecule that become mobile [1]. Each "bead" is equivalent to a bond about which motion to various conformational isomers is possible or a contribution of the molecule as a whole [2] (11.3 J K^{-1} mol^{-1} per bead, and about twice to three-times this amount for the overall, large molecule). From the DSC data of the amorphous phase one concludes, thus, that in each branch of the MOCPM molecule there are only about five mobile bonds out of the seven visible in the structural formula, above. On the other hand, one can also use the entropy of fusion to estimate the gain of conformational mobility in going from the (rigid) crystal to the melt. The entropy of fusion measured by DSC; converted to 100% crystallinity was 169 J $K^{-1}mol^{-1}$, corresponding to only about three bonds per branch of the molecule that become conformationally disordered and mobile on melting (after correction for translational and orientational gain of entropy of the molecule as a whole). The heat capacity study indicated that there is no gain of conformational entropy outside the transition region, leaving the entropy deficit unexplained. In the present paper this problem will be resolved.

The solid state NMR and X-ray study reported in this paper was designed to clarify the molecular order and molecular motion in the crystal and melt of MOCPM and find an explanation of the DSC measurements. Such unique combination of thermal analysis, solid state NMR, and X-ray techniques has proven a powerful method in the investigation of the thermal transition behavior and molecular origin of large-amplitude motion in small and large organic molecules. Various cases of deficit of entropies of transition could be documented [3–20], and will be used in this research to identify the behavior of MOCPM. A simple molecular mechanics software was used throughout to model the molecular structure suggested by the experiments.

Experimental

NMR experiments

The solid state ^{13}C NMR spectra were measured with a Nicolet NT-200 NMR spectrometer equipped with a Doty Scientific magic-angle spinning (MAS) probe, operating at 50.31 MHz and 200.07 MHz for ^{13}C and ^{1}H, respectively. Temperature control was obtained using the standard Nicolet controller. Rotors (cylindrical sample container, 5 mm in diameter) were supplied by Doty Scientific and machined from single crystals of Al_2O_3 (sapphire). The end caps used for the rotor were made from brown plastic Vespel® (Registered trademark for a DuPont polyimide). The sample was rotated with nitrogen gas at 4.5 kHz at the magic angle. Prior to each measurement, probe tuning and matching are performed to minimize the reflected *rf* power.

The conventional one-pulse of ^{13}C NMR with two-level decoupling of protons (BILEV) was also performed. It was used to obtain the spectra of the

mobile molecules in the melt and in the amorphous fraction above the glass transition temperature. The pulse width used for ^{13}C was 3.9 μs, corresponding to an 85° flip angle, and the recycle delay between two successive pulse sequences was 2.0 s. These conditions ensure the elimination of resonances from rigid carbon atoms in the well-ordered region having long spin-lattice relaxation times (T_1). The ^{13}C spectra of the rigid materials were obtained using the methods of cross-polarization, high-power proton decoupling, and magic-angle sample spinning (CP-MAS). The signals from the liquid-like amorphous phase will be in this case suppressed because the dipolar interaction between protons and carbons is diminished by the fast molecular motion, so that no cross-polarization can occur. The CP-MAS experimental parameters were as follows: contact time, 2.0 ms; proton 90° pulse, 5.0 μs; recycle time 3 s; number of transients, 200.

The dipolar dephasing pulse sequence, a slight modification to the standard CP-MAS, was used to suppress the signals from the carbons with strong dipolar coupling to nearby protons. In the more rigid region, the molecules show stronger dipolar coupling. This experiment was carried out by inserting a dephasing delay, τ, following C–H cross-polarization and prior to signal acquisition (when $\tau = 0$ μs, the dephasing experiment is identical to the standard CP-MAS) [21]. The dephasing experiment was performed on the as-delivered (highly crystalline) sample at $T = 296$ K for the confirmation of the chemical shift assignment, as is described in the Results section. The spin-lattice relaxation times (T_1) were measured at the temperature above the melting point of the sample by using magic-angle spinning and high-power proton decoupling, with the inversion-recovery (IR) method [22]. Delay times of 0.000 01 to 1.5 s were used while the number of transients were typically 200. Proton saturation was applied during the variable delay time. The ^{13}C 90° and 180° flip angles occur at 4.1 and 8.2 μs, respectively. The recycle time of the IR was 3 s. The spectra for relaxation measurements were obtained by repeated cycling through the different delay times, each time adding in a few free induction decays. This method of experiment interleaving eliminates possible errors from long-term changes, such as spinner instability, amplifier drop, etc. When plots of the data show single-exponential behavior, the T_1 values were taken from a least-squares fit of the experimental data points.

The ^{13}C chemical-shift reference was set using hexamethylbenzene (17.36 ppm for the methyl carbon relative to tetramethylsilane) prior to the experiment. The field drifting of the spectrometer was estimated to be less than 0.05 ppm during an experiment.

For the variable temperature measurements, the instrument temperature calibration was done with the liquid ethylene glycol. Known change of the separation of the two proton resonances ($\Delta\delta$) relate with the change of temperature [23].

The X-ray diffraction measurements

The X-ray measurements were carried out on a Scintag PAD-X powder diffractometer using reflection geometry. The diffractometer was equipped with a Peltier-cooled solid-state detector and used Cu radiation. Temperature control was accomplished with resistive heating of a 20×12×2 mm^3 sample holder of aluminum, balanced by circulating coolant from a cold-temperature bath. The sample and sample holder were isolated in a high-temperature chamber filled with N_2 gas. For the semicrystalline diffraction pattern, the sample was used as received (*i.e.* well crystallized) and packed in the aluminum sample holder with a free, flat sample surface. For the liquid measurements the sample was fused at 313 K and cooled to 290 K. The diffraction pattern of the supercooled sample was measured in the same Al sample holder. Once molten, the sample remained liquid for several days before crystallizing [1], providing ample time for completing the X-ray measurements on the liquid. Care was taken to ensure identical sample geometry and environmental conditions for the measurements of the semicrystalline and liquid diffraction patterns.

The diffraction patterns were corrected for polarization, absorption [24], sample geometry [24], incoherent (Compton) scattering [25], monochromator discrimination [26], and multiple scattering [27]. After correction the patterns were normalized to the self-scattering [28] expected from the MOCPM molecule to permit quantitative comparisons of the patterns.

Samples

The sample of MOCPM is an Exxon Inc. Chemical product of high purity and was analyzed as obtained. No impurities could be detected by NMR. For storage, the sample was hermetically sealed and kept at room temperature. Because of the low melting temperature this is an annealing condition, *i.e.* as-delivered, the sample was crystalline and was then measured with and without thermal pretreatment. To recover the semicrystalline state after melting took annealing at room temperature of more than three days.

Modeling of the molecule

To estimate the energetics of the various conformations a simple computer modeling was done. The software used was Molecular Modeling Pro® (WindowChem, Rev. 1.19) by NorGwyn Montgomery Software Inc. Figure 1 shows the approximately energy minimized structure of the molecule. For analysis of the rotation, each bond was rotated singly and, if needed, in conjunction with the neighboring bond. Major steric hindrances from further removed parts of the molecule were eliminated where necessary by constructing model compounds. For comparison, the CH_3-groups were sometimes averaged by giving them the chlorine radius.

Results

Peak assignments for the ^{13}C NMR spectrum

The molecular structure of the MOCPM has been shown in the Introduction with the numbering of the distinguishable carbon atoms. The peak assignments are made based on the liquid spectrum (melt) with and without proton decoupling, as shown in Fig. 2. The bottom spectrum is the BILEV spectrum with proton decoupling at $T = 323$ K (above the melting point). Preliminary peak assignments can be made by comparing the chemical shift value in this spectrum to the standard spectra of compounds which have similar molecular segments or functional group to those of MOCPM [29]. The top spectrum in Fig. 2 is the BILEV spectrum without proton decoupling, also at $T=323$ K. This spectrum can give the information of how many protons are directly attached to each individual carbon, because one ^{13}C resonance can be split into a group of lines due to the spin-spin interaction between the observed carbon and the protons directly attached to it. This spectrum can, thus, be used to confirm the preliminary assignment and complete the peak assignment. In addition, the CP-MAS spectrum at $T=296$ K with a dephasing time 30 μs (as shown Fig. 3, the

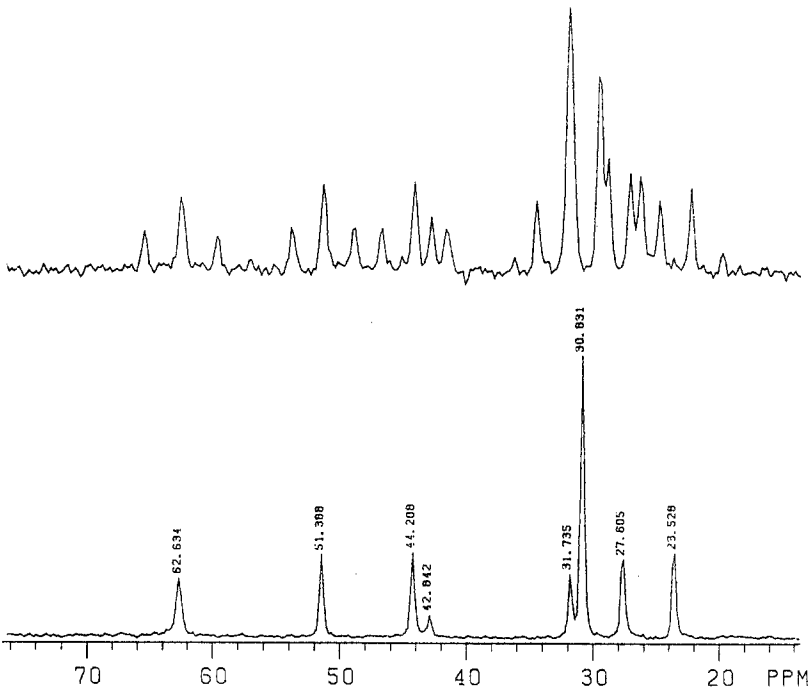

Fig. 2 Expanded BILEV spectra at $T=$ 323 K. The marked peaks correspond, from left to right to C-2, -7, -4, -1, -8, -9, -5, and -6. (The C-3 peak at 171.7 ppm is to the left of the scale, the top spectrum is taken without proton decoupling, the bottom one with decoupling.)

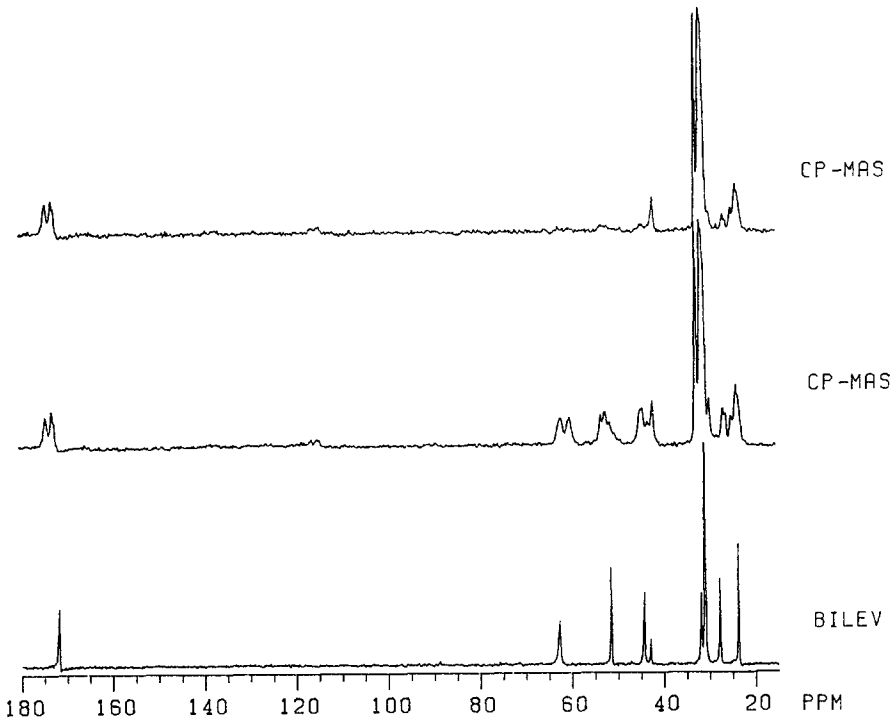

Fig. 3 Two CP-MAS spectra at T = 296 K. The top curve is a CP-MAS spectrum with a dephasing time τ = 30 μs, the center curve, without. At the bottom the BILEV spectrum is repeated as reference

top spectrum) is used to confirm the peak assignments of the carbon atoms without directly attached protons. The peak of the carbons without protons can survive the spin-dipolar dephasing, while the peaks of the carbons with protons will have decayed during the dephasing. Combining all methods enables the peak assignments for all carbon atoms of MOCPM. The ^{13}C chemical shift values δ are given in Table 1.

Table 1 Chemical shift in the melt (in ppm; T=323 K)

C-1	C-2	C-3	C-4	C-5	C-6	C-7	C-8	C-9
42.8	62.6	171.7	44.1	27.6	23.5	51.3	31.7	30.8

^{13}C chemical shifts and spin-lattice relaxation times

The CP-MAS spectra with variable temperature are plotted in Fig. 4. It is interesting to note that below the melting temperature (T =304 K), the CP-MAS spectra show a dual-peak pattern for each carbon atom (except for the

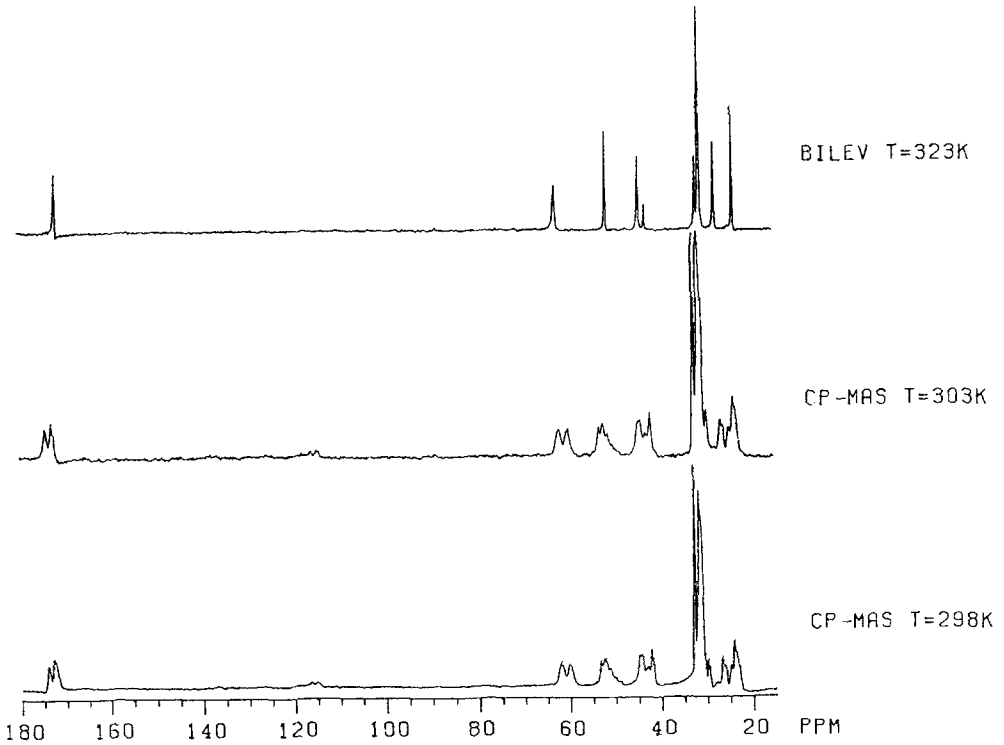

Fig. 4 Crystalline CP-MAS spectra at 298 and 303 K. The BILEV spectrum on the top is used as reference

central carbon C-1), and the chemical shift values are not changed as the temperature increases from T =298 to 303 K. When the temperature reaches 306 K, the CP-MAS signal completely disappears, only the BILEV signal is retained. This indicates that the sample is fully molten at this temperature and the molecules are too mobile to give a CP signal. The chemical shift δ for each carbon atom in the crystal phase is listed in Table 2.

Table 2 Chemical shift in the crystal (in ppm; T=298 K)

C-1	C-2	C-3	C-4	C-5	C-6	C-7	C-8	C-9
41.9	60.0	174.0	42.9	26.0	24.8	53.1	32.5	29.7
41.9	61.9	172.3	44.1	26.6	23.0	52.2	31.5	30.9

The BILEV spectra at selected temperatures are shown in Fig. 5. These signals are contributed by the (mobile) amorphous portions of the sample between glass transition and melting transition temperatures. For reference, the ^{13}C spectrum of the melt is plotted on top. The fact that the chemical shift of each

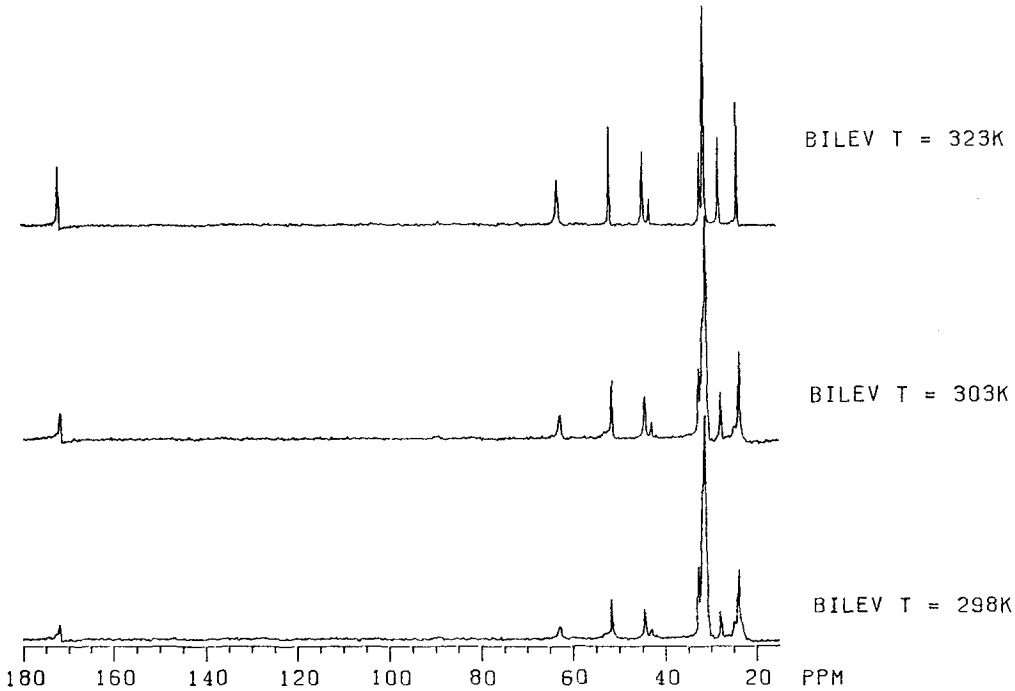

Fig. 5 The dependence of the BILEV spectra on temperatures

carbon atom in the BILEV spectra below and above the melting temperature is the same is evidence that the molecules in the amorphous phase have the same disorder as is found in the melt.

The spin-lattice relaxation time T_1 of each carbon atom in the melt was measured at $T = 323$ K. The measured T_1 values are listed in Table 3. Their relative errors are less than 20%. The interpretation of the data are given in the discussion section.

Table 3 The T_1 values in the melt (in seconds; T=323 K)

C-1	C-2	C-3	C-4	C-5	C-6	C-7	C-8	C-9
0.48	0.062	0.97	0.13	0.23	0.54	0.20	2.6	0.48

The X-ray data

The diffraction patterns for the semicrystalline and liquid materials are shown in Fig. 6. Both diffraction patterns were normalized to the self-scattering of one MOCPM molecule (the curve dropping-off smoothly with scattering angle 2θ). This enables direct comparisons between the liquid and semicrystalline

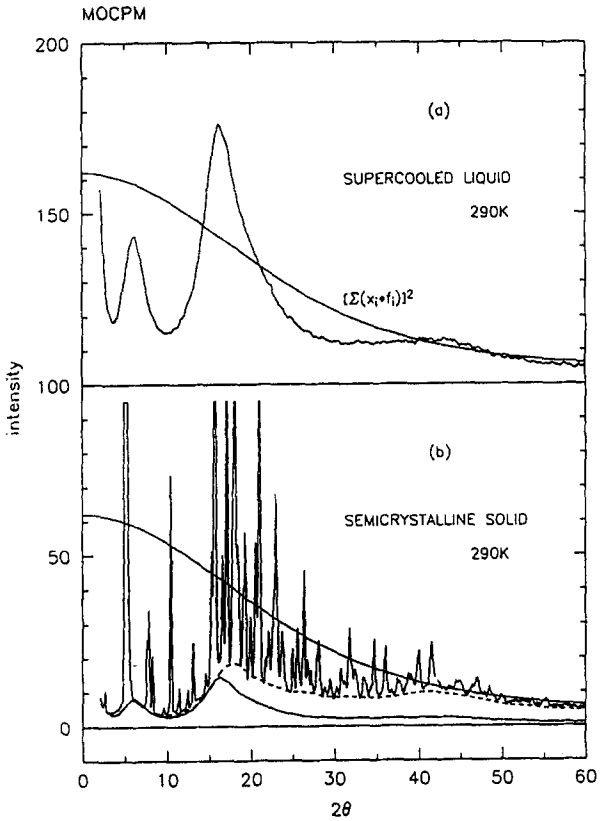

Fig. 6 Wide angle X-ray diffraction pattern of MOCPM. (a) The supercooled liquid at 290 K. (b) The semicrystalline material at 290 K; the dashed curve delineates the non-crystalline scattering; the lower smooth curve is the scaled supercooled liquid pattern. Both patterns are normalized to the self-scattering from MOCPM, the sum of the weighted scattering factors

patterns. The diffraction pattern of the supercooled liquid is typical for an organic liquid with a characteristic strong peak at $2\theta = 16.3°$, representative of intermolecular carbon-carbon contact distances of about 0.4–0.5 nm. An unusual, though well understood, feature of the liquid diffraction pattern is a pronounced second peak at low 2θ angles ($\approx 6.5°$). This peak arises from the average intermolecular distance between the bulky molecules in the liquid (Fig. 1).

The semi-crystalline diffraction pattern in Fig. 6 shows a substantial amount of diffuse, non-crystalline scattering, indicated by the dashed line. Attempts to decrease the amount of non-crystalline scattering by annealing were not successful. For comparison, a scaled version of the liquid scattering is superimposed on the semicrystalline scattering pattern. Clearly a second disordered component can be observed besides the liquid-like scattering.

Discussion

The amorphous phases

The X-ray data reveal that the main peak in the supercooled liquid arises from the intermolecular C···C contact distances (or contact distances between carbon atoms on different arms of the same molecule). This peak usually corresponds to a 0.4–0.5 nm distance. For the liquid MOCPM this peak corresponds to a separation of 0.54 nm, a distance indicating a less dense packing than for typical organic fluids and polymers. This is probably due to the bulkiness in the branches of the MOCPM (=O and $-CH_3$ groups).

The so-called "pre-peak" at 6.5° corresponding to ≈1.36 nm, is a measure of the average intermolecular center-to-center distance of the bulky molecules in the liquid. This distance can be compared to those measured in melts of tetra-*n*-alkylammonium halides (TAAX), analyzed in our laboratory [30] (the numeral gives the length of the branches in number of C-atoms, the letters the cation; 7Br is, for example, tetra-*n*-heptylammonium bromide):

5I	1.12 nm	5Br	1.16 nm
6I	1.30 nm	6Br	1.31 nm
7I	1.40 nm	7Br	1.44 nm
		8Br	1.55 nm
		10Br	1.79 nm

Clearly, the center-center distances increase with increasing size of the tetraalkyl ammonium ion. For MOCPM, each arm has a backbone chain length of eight, and should be compared to 8Br and 8I which each have a separation of about 1.5 nm. The comparison is complicated by the presence of the anion in the TAAX, which will serve to expand the average center to center distance in the melt. The center-center distance in MOCPM can also be compared to the molecular dimensions given in Fig. 1. Clearly, the measured distance of 1.36 nm in the melt indicates that the molecule collapsed to some degree due to a higher number of *gauche* conformations as indicated by the NMR data, and there can also be significant interpenetration of the arms from different molecules, *i.e.* a "nesting" of molecules.

Figure 6 shows that a considerable amount of the same amorphous (liquid) X-ray scattering remains in the semicrystalline phase. Additional non-crystalline scattering can be seen in the figure and will be discussed below. Similarly Figs 4 and 5 show that by solid state NMR both BILEV and CP-MAS spectra are detectable in the temperature range from the glass transition temperature (219 K) to the melting point (304 K). This indicates the existence of two phases in this temperature range with distinguishable molecular mobilities. In the amorphous phase the molecules are sufficiently mobile that the BILEV signal is detectable only, while in the crystalline phase the molecules are so rigid that

only the CP-MAS signal is obtainable. The difference of the BILEV and CP-MAS patterns (at the same temperatures) prove that the molecular ordering in these two phases is quite different.

The peak positions of all carbons of the amorphous phases shown in Fig. 5 do not change as the temperature increases from $T = 298$ K to $T = 323$ K (above the melting point). This means that the intramolecular conformations of the molecules in the amorphous phase below the melting temperature are the same as in the melt. The BILEV spectra at $T = 298$ K and $T = 303$ K show a small shoulder at the peaks attributed to C-9 and C-6 (Table 1). These shoulders originate from signals of the same carbons in the crystalline phase. It is well known that methyl groups in the solid state are quite mobile, even at very low temperatures. In the present case they are even sufficiently mobile to be observed by the BILEV technique.

Conformational order and mobility as derived from NMR and modeling

A. Basic principles of chemical shift and γ-*gauche* effect

The chemical shift of a ^{13}C NMR spectrum depends on both, inter- and intra-molecular interactions. The former changes with the packing of molecules, and the latter is influenced by the molecular conformation. The changes in intramolecular conformation are the most important influences on the ^{13}C chemical shift (δ) [31, 32], while the intermolecular effects are of secondary importance.

The δ of a given ^{13}C is influenced by substituents in the α-, β-, and γ-positions relative to the observed carbon. The α- and β-substituents have fixed intramolecular contributions to the δ value of the observed carbon as long as the chemical structure of the molecule is fixed. The γ-substituent effect has a conformational origin [31, 32]. Marking the observed carbon as °C, and its γ-substituent $^{\gamma}X$, the structure can be written as $^{\circ}CH_2–CH_2–CH_2–^{\gamma}X$. In the present case the γ-substituent may be C or O. One can see that the distance between $^{\circ}CH_2$ and $^{\gamma}X$ varies with the rotation angle about the central bond. Therefore, the change of the ^{13}C δ can be linked to changes in the conformation (or rotational state). For a ^{13}C to be more shielded by a γ-substituent, $^{\gamma}X$, it has been suggested that the °C and $^{\gamma}X$ must be in a *gauche* arrangement. The effect of such γ-*gauche* shielding has been evaluated to be: $\gamma_{C-C} = -5.2$ ppm and $\gamma_{C-O} = -7.2$ ppm [32]. In the melt or in solution, the rotating C–C bonds are expected to have a population of about 40% *gauche* conformation, a value based on an energy difference of about 2.8 kJ mol^{-1} between *gauche* and *trans* conformations and an approximate temperature of 400 K [33]. Accordingly, one expects after a transition from a fully ordered, all-*trans*, conformation to one with 40% of *gauche*, that the δ of the ^{13}C decreases (becomes more shielded) by $\Delta\delta = 2 \times (0.4) \times (-5.2)$ ppm $= -4.16$ ppm for a C-atom in the γ-position. The factor of

two accounts for the situation that two γ-substituents may exist, one on each side of the °C. If only one of the two γ-substituents has changed, Δδ is expected to be only –2.08 ppm. Similarly, if neither of the γ-substituents changes its spatial relationship with respect to °C, Δδ is zero. Based on this argument, the changes in intramolecular conformations on going from the crystal to the melt can be discussed.

B. The change of the NMR spectrum on melting and its link to conformation and mobility

The CP-MAS NMR spectra of the crystal phase (Table 2, Fig. 4) show dual patterns for each but carbon atom 1. From the top CP-MAS trace in Fig. 3 one can see that after long enough dephasing to eliminate the overlapping signals contributed from C-4, there is only a single peak associated with C-1. This indicates that in the rigid phase all C-1 atoms have the same molecular enviroruneut. *i.e.*, there is only one type of C-1 carbons in the crystal, in contrast to all others. Comparing Table 1 with the data from the melt (Table 1, BILEV spectra, Fig. 5), one finds that in the dual peak pattern from the crystal, one set of peaks has chemical shifts close to those of the melt, while the others are different by about 1.5–2.5 ppm.

For the peaks with chemical shifts close to the melt (bottom row in Table 2), the differences before and after isotropization (final melting) are less than 1 ppm. Such small changes in chemical shift are normally due to different packing effects between the solid and liquid states. Therefore, the atoms contributing to these signals must have the same intramolecular conformation in the crystal and in the melt, *i.e.* no further conformational disorder is introduced by melting.

For the peaks with different chemical shifts than in the melt (top row in Table 2), one should be able to relate the changes Δδ to conformational motion about specific bonds initiated on fusion. The analysis shows complications in interpretation of the γ-*gauche* effect due to the multiple methyl groups. Spin-lattice relaxation times are, thus, needed for resolution of the question of mobility. In brief, all ordered bonds in the crystal become mobile, except the two that are even rigid in the melt (see above). The details are as follows:

The chemical shift of C-1 should be influenced by the conformational motion about the bond C-2–O, but note that there are four $^{\gamma}$C atoms for this quaternary carbon and a close approach of C-3 may not be possible. The change in δ for ΔC-1 = +0.9 ppm (the + sign means down-field shift) is, thus, in accord with the quaternary nature of C-1. It is too small to be assigned to a sizeable γ-*gauche* effect. Rotational motion about C-2–O would also cause changes in ΔC-3 (to be discussed below). From its discussion and evidence from spin-lattice relaxation time T_1 and estimates of the rotational potential it will be concluded that C-2–O is, indeed, permitting rotation in the melt.

For C-2, rotational motion of the O–C-3 bond of the same molecular branch and the C-1–C-2 bond of the three other molecular branches can contribute to ΔC-2. The observed value ΔC-2 = +2.6 ppm is in accord with some γ-*gauche* effect, but in direction *gauche→trans*. In the O–C-3 bond, the electronic conjugation between O–C-3 and C=O make the potential barrier for rotation about O–C-3 sufficiently high to hinder rotation [33]. Molecular mechanics calculations for MOCPM as shown in Fig. 1 yield for this bond a potential energy barrier for rotation of about 45.7 kJ mol^{-1} if no major steric hindrance of other parts of the molecules occurs. This value is similar to the barrier to rotation in linear, all-*trans* paraffinic esters (44.8 kJ mol^{-1}) and is too high to be overcome by thermal motion at 304 K. Thus, to discuss the value ΔC-2, one needs to consider only rotation about the three C-1–C-2 bonds in the branches not part of the C-2 under discussion. A *gauche*-bond brings the O-atom of one of the neighboring branches in close proximity with C-2. Crystals of TAAX contain a quaternary N instead of a C-atom. For these crystals the structure is known [34] and may serve as a model for MOCPM. Two of the C-1–C-2-bonds are *trans*, while one is *gauche* relative to the C-2 in question. The positive value of ΔC-2 suggests that the crystal keeps C-2 in a more frequent *gauche* position than in the melt (relative to the O atoms in the other branches). On melting, the four branches become mobile, but on average, the molecule opens up from two *trans* and one *gauche* conformation to only 0.4 *gauche* bond in the melt (0.36×7.2 = 2.68 ppm, the observed ΔC-2). Each C-2 would then have a "normal" *gauche-trans* relationship with one of the three branches, while the other two extend away in a *trans* conformation similar as shown in Fig. 1 with the hidden chain bending towards C-2 in the forward chain. Molecular mechanics computations indicate that by cooperative rotation about bonds C-1–C-2 and C-2–O paths are available with barriers as low as a few kJ. The TAAX molecules, in contrast to MOCPM, remain rigid on melting, most likely caused by the cation charge distributed about the quaternary nitrogen.

Conformational motion about C-2–O and C-4–C-5 bonds can influence the change of δ of C-3. From models one can easily see that C-6 in the $-CH_3$-group attached to C-5 is *gauche* relative to C-3 when the C-4–C-5 conformation makes C-7 *trans* relative to C-3, *i.e.* there is always a certain *gauche* effect on C-3, even when C-4–C-5 arranges the backbone in an all-*trans* conformation. The rotation about C-2–O is also not straightforward. It results in an approach of C-3 to C-1 that was shown above to be sterically hindered. The observed ΔC-3 = –2.3 ppm is, thus probably not a "normal" γ-*gauche*-effect, but needs a more detailed conformational analysis. Fortunately, the mobility about the C-2–O-bond can be derived without difficulties from the T_1 measurement, below. Molecular mechanics calculations of rotation about this bond also show no strong hindering to rotation as long as the major interference between the dif-

ferent branches of the molecule are avoided by cooperative rotation about other bonds.

The next CH_2-group has a ΔC-4 $= +1.2$ ppm, which is too small (and in a *gauche→trans* direction) to be assigned as a γ-*gauche*-effect, indicating that both, the O–OC-3 and the C-5–C-7 bonds do not change their conformation significantly on melting. The ΔC-2 analysis already indicated immobility of O–OC-3 because of its double-bond character. The immobility about C-5–C-7 can be understood from inspection of a molecular model. The steric hindrance between the methyl group C-6 and the three methyl groups C-9 is sufficient to forbid rotation about C-5–C-7. Molecular mechanics estimates of rotation about this bond show no path of low energy and a *trans* conformation for the bond.

The two bonds related to ΔC-5 are C-3–C-4 and C-7–C-8. Starting with C-3–C-4, one can see from a molecular model that the *trans* conformation of the backbone brings C-5 halfway between the two *gauche* positions of the =O atom of C-3, while the *gauche* backbone brings it close to the O-atom of O–C-3. It may thus be that rotation about C-3–C-4 actually reduces the O-interaction somewhat (note that δ is 7.2 for O γ-*gauche* to C and ΔC-5 $= +1.6$). Meanwhile, the rotation about C-7–C-8 cannot strongly influence ΔC-5 because one of the three C-9 CH_3 groups in the γ position is always *gauche* relative to C-5. One concludes that the C-3–C-4 and the C-7–C-8-bond may both undergo conformational motion in the melt even though they do not cause a large ΔC-5. The molecular mechanics calculations show a barrier to rotation of bond C-3–C-4 of only 6.7 kJ mol^{-1} when using the conformation shown in Fig. 1. Bond C-7–C-8 is more difficult to estimate with the available simple software. Low energy paths can be obtained for the *trans* conformation for the rather immobile bond C-5–C-7. Averaging the CH_3-groups to chlorine radii leads to potential energy barriers of about 10 kJ mol^{-1}, still in accord with mobility in the melt.

The -1.3 ppm value of ΔC-6 is coupled to possible rotations about C-5–C-7 and C-4–C-5. The discussion of ΔC-4, above, revealed that C-5–C-7 is immobile even in the melt. This leaves the rotation about C-4–C-5 for the discussion of the chemical shift. The small γ-*gauche* effect seems to indicate that the *trans* concentration in the melt may remain higher than normal ($>60\%$), a fact that may well be connected to the bulky nature of the molecule. Molecular mechanics calculations provides a minimum energy path with an activation energies of about 13 kJ mol^{-1} as long as the rigid C-5–C-7-bond remains *trans*.

For C-7, only rotating about C-4–C-5 can cause a γ-*gauche* effect. The value of ΔC-7 is -1.8 ppm. The same conclusion as reached for ΔC-6 should apply. Rotation about C-4–C-5 bond leads to a somewhat higher *trans* to *gauche* ratio than normal.

The value of ΔC-8 can only be related to the C-5–C-7 bond, which was shown before to be immobile. This agrees with ΔC-8 $= -0.7$ ppm, a small $\Delta\delta$ value.

Finally, the value of ΔC-9 $=-1.1$ ppm has been attributed to a packing effect, since the rotation about the C-7–C-8 bond does not influence ΔC-9 due to the symmetry of the three identical C-9 atoms. The rotational motion of C-7–C-8, being likely according to the molecular mechanics calculations summarized above, will be derived from the study of T_1.

C. Spin-lattice relaxation times T_1 in the melt

The spin-lattice relaxation times T_1 of Table 3 measured at a temperature of 323 K were used to confirm the rotational motion about the bonds of MOCPM in the melt as derived from the chemical-shift discussion. Basically, since the external magnetic field-strength is in the range of MHz, the frequency of motion detectable by this measurement is also in the MHz range. This frequency-range covers normally the large-amplitude conformational motion. According to the spin-lattice relaxation theory, in the liquid state (melt) [34], T_1 is approximately proportional to the reciprocal of the correlation time τ. The larger T_1, the faster is the motion. Furthermore T_1 of each carbon atom has two contributions: first, the orientational motion of the whole molecule, second the conformational motion about the individual chemical bonds [35]. Assuming that the orientational motion of the whole molecule gives, on average, the same contribution for each atom, the differences in T_1 between two carbon atoms connected by a chemical bond indicates the mobility about this bond. Applying this interpretation to the data of Table 3 gives the following interpretation:

Starting from C-2, the T_1 values of carbon atoms with similar local environment, for example C-2, C-4 and C-7, increase from C-2 to C-7. This indicates that the conformational motion of each C–C-bond becomes faster when going from the inner-most bond to the end of the branch. The same conclusion is reached for C-1 and C-8.

Additionally the T_1 value of C-5 (0.23 s) is so close to T_1 of C-7 (0.20 s) to confirm the rigidity of the C-5–C-7-bond observed from the chemical shift changes and suggested by the molecular modeling attempts. On the other hand, the difference in T_1 between C-1 and C-2 is evidence of some conformational motion about the C-1–C-2 bond. The quite different T_1 values between C-2 and C-3 indicate also the mobility of C-2–O bond (if the C-2–O–C-3–O were a rigid rotor, T_1 of C-2 and C-3 would have to be the same).

The semicrystalline state

Several computer programs were used to try to index the crystalline X-ray scattering to obtain the unit cell. These were not successful. The very strong peak at $2\theta \approx 5.2^\circ$ is, however, likely a low order reflection, related to planes that contain the MOCPM molecules. The *d*-spacing of this peak of 1.70 nm, is simi-

lar to the center-center distance in the liquid. The small peak at $2\theta \approx 2.6°$ indicates that the unit cell size is, at least in one dimension, 3.4 nm or larger.

The diffraction pattern of the semi-crystalline sample shows appreciable amounts of non-crystalline scattering, as indicated by the dashed line in Fig. 6. The diffuse scattering is concentrated at 2θ angles higher than in the liquid sample, as can be seen from the overlay of a scaled liquid pattern. The peak in the non-crystalline scattering in the semi-crystalline material occurs at $\approx 17.7°$ *vs.* 16.3° in the liquid. This is not the usual temperature effect between liquid and solid, since the two patterns were taken at the same temperature. In addition, there is considerably more scattering intensity in the semicrystalline material than in the liquid at higher diffraction angles. Thus, the nature of the non-crystalline material in the semi-crystalline solid differs from that in the liquid.

The areas corresponding to the crystalline and total non-crystalline scattering from the semi-crystalline sample are 56% and 44%, respectively. If one assumes that a portion of the disordered material in the solid is liquid-like (*i.e.*, amorphous), as would be suggested by the remaining small glass transition in these materials, the non-crystalline scattering can be further divided into liquid-like scattering and "other" non-crystalline scattering. The maximum amount of liquid-like amorphous scattering is 16% in good accord with the crystallinity estimated from DSC [1]. The value was chosen by keeping the liquid pattern overlay below the Bragg peaks. This leaves a minimum of 28% of "other" non-crystalline scattering. This "other" non-crystalline scattering might come from the conformationally disordered parts of the molecules in the crystallites.

The NMR data have shown that 20 bonds are able to rotate in the melt. The DSC measurements find, however only 13 from an analysis of the entropy of fusion [1]. Assuming that seven of the bonds (35%) of each crystallized molecule in the crystal remain disordered on crystallization accounts for the 28% "other" noncrystalline scattering and also furnishes a reason for the double peaks of similar magnitude in the NMR spectra of the crystals.

It is remarkable that the (scaled) liquid pattern fits the non-crystalline pattern in the solid very well up to $2\theta \approx 15°$, indicating that the diffuse scattering from the "other" disorder begins at 15° and is more or less constant at higher angles. The shape of this diffuse scattering from the "other" disorder is similar to the diffuse scattering seen in long-chain conformationally disordered TAAX [33] (long meaning alkyl chains with more than 4 methylene units). In a disordering transition of the TAAX the tetra-*n*-alkylammonium ions as a whole remain on lattice sites, with only the alkyl chains gaining conformational disorder. This is precisely the picture emerging for MOCPM (with the exception that in MOCPM there are additional regions of ordinary amorphous, liquid-like material, not present in TAAX).

A simple model of crystallization can explain the observed unique crystallization behavior of MOCPM that consists of slow, incomplete crystallization to

limits of 16% amorphous, 28% conformationally disordered, and 56% crystalline. It is well known that only a specific chiral center fits into a given crystal [36]. Assuming that the four centers in MOCPM occur randomly, there are 12.5% of the molecules that agree in only one chain with a given configuration and similarly 12.5% that agree with all four. Assuming that the former molecules remain amorphous and the latter form the basis of the crystals accounts for only 25% of the material. Half of the remaining molecules have one branch not fitting into a given configuration for a crystal and the other half have two. If the molecules with one or two branches with wrong configurations remain conformationally disordered, they would account for 28% of disorder. The total ordered branches of the molecules would then make 56%. These percentages are close to the observed values and would also give a reason why further crystallization and ordering is inhibited.

Conclusions

- The X-ray diffraction pattern of the supercooled liquid MOCPM indicates a typical organic liquid made up of bulky, nested molecules.
- By conformational analysis based on the ^{13}C NMR spectra of the melt and the crystal, and by molecular mechanics calculations it was possible to show that rotational motion is restricted for the O–OC-3 and the C-5–C-7 bonds. This conclusion agrees quantitatively with the overall increase in C_p at the glass transition.
- The semicrystalline solid MOCPM is about 56% crystalline, 16% liquid-like amorphous, and 28% conformationally disordered crystalline, in quantitative agreement with the entropy deficit discovered by analysis of the melting transition by DSC and the small glass transition observed in semicrystalline samples.
- The conformational disorder in the crystal in some of the branches of the molecules involves all but the center atom C-1.
- Below the isotropization temperature there is no gradual change in conformational disorder observed by ^{13}C NMR, in agreement with the heat capacity measurement.
- If possible, the fully crystalline structure of MOCPM should be determined to find the nature of the disorder in the crystalline regions. At present one can speculate that an orderly packing is interrupted by the presence of random stereo isomers at the C-5 atom. This would be the first example of a crystal of a small molecule that can accommodate molecules with only two or three of its branches configurationally correct. An incorrect chiral center leaves the branch disordered and mobile (conformationally disordered crystal, condis crystal [37]). A simple statistical analysis agrees with the observed limiting percentages of disorder.

The work of M.P. was supported by the Exxon and Engineering Company New Jersey, under Contract #CO7-C-3185. The ATHAS group is supported by the Division of Materials Research, National Science Foundation, Polymers Program, Grant # DMR 90-00520 and the Division of Materials Sciences, Office of Basic Energy Sciences, U. S. Department of Energy, under Contract DE-AC05-84OR21400 with Lockheed Martin Energy Systems, Inc.

References

1 M. Pyda, M. Varma-Nair, W. Chen, H. S. Aldrich and B. Wunderlich, J. Thermal Anal., preceding paper.
2 B. Wunderlich, "Thermal Analysis." Academic Press, Boston, MA, 1990.
3 B. Wunderlich, M. Möller and H. G. Wiedemann, Mol. Cryst. Liq. Cryst., 140 (1986) 211.
4 H. G. Wiedemann, J. Grebowicz and B. Wunderlich, Mol. Cryst. Liq. Cryst., 140 (1986) 219.
5 M. Y. Cao, J. Wesson, K. Loufakis and B. Wunderlich, Mol. Cryst. Liq. Cryst., 140 (1986) 231.
6 M. Möller, D. Oelfin and B. Wunderlich, Mol. Cryst. Liq. Cryst., 173, (1989) 101.
7 A. Xenopoulos, J. Cheng, M. Yasuniwa and B. Wunderlich, Mol. Cryst. Liq. Cryst., 214 (1992) 63.
8 J. Cheng, A. Xenopoulos and B. Wunderlich, Mol. Cryst. Liq. Cryst., 220 (1992) 127.
9 J. Cheng, Y. Jin, G. Liang, B. Wunderlich and H. G. Wiedemann, Mol. Cryst, Liq. Cryst., 213 (1992) 237.
9a J. Cheng, Y. Jin, B. Wunderlich, S. Z. D. Cheng, M. A Yandrasits, A. Zhang and V. Percec, Macromolecules, 25 (1992) 5991.
10 M. A. Yandrasits, S. Z. D. Cheng, A. Zhang, J. Cheng, B. Wunderlich and V. Percec, Macromolecules, 25 (1992) 2112.
11 J. Cheng, A. Xenopoulos and B. Wunderlich, Mol. Cryst. Liq. Cryst., 220 (1992) 105.
12 Y. Jin, J. Cheng, B. Wunderlich, S. Z. D. Cheng, M. A. Yandrasits and A. Zhang, Polym. Adv. Technol. 5 (1994) 785.
13 J. Cheng, A. Xenopoulos and B. Wunderlich, Mol. Cryst. Liq. Cryst., 225 (1992) 337.
14 A. Xenopoulos, J. Cheng and B. Wunderlich, Mol. Cryst. Liq. Cryst., 226 (1993) 87.
15 Y. Jin, J. Cheng, M. Varma-Nair, G. Liang, Y. Fu, B. Wunderlich, X.-D. Xiang, R. Motovoy and A. K. Zettl, J. Phys. Chemistry, 96 (1992) 5151.
16 J. Cheng, Y. Jin, W. Chen, B. Wunderlich, H. Jonsson, A. Hult, and U. W. Gedde, J. Polymer Sci., Part B: Polymer Physics, 32 (1994) 721.
17 J. Cheng, W. Chen, Y. Jin and B. Wunderlich, Mol. Cryst. Liq. Cryst., 241 (1994) 299.
18 Y. Jin, A. Xenopoulos, J. Cheng, W. Chen, B. Wunderlich, M. Diack, C. Jin, R. L. Hettich, R. N. Compton and G. Guiochon, Mol. Cryst. Liq. Cryst., 257 (1995) 235.
19 J. Cheng, Y. Jin, A. Xenopoulos, W. Chen, B. Wunderlich, M. Diack, R. N. Compton and G. Guiochon, Mol. Cryst. Liq. Cryst., 250 (1995) 359.
20 Q. Wang, A. Xenopoulos and B. Wunderlich, Mol. Cryst. Liq. Cryst. 264 (1995) 115.
21 S. J. Opella and M. H. Frey, J. Am. Chem. Soc." 101 (1979) 5854.
22 E. D. Becker, "High Resolution NMR." Second ed., Academic Press, New York 1980.
23 A. L. Van Geat, Anal. Chem., 42 (1970) 697.
24 H. A. Levy, P. A. Agron and M. D. Danford, J. Appl. Phys., 30 (1959) 2012.
25 D. T. Cromer and J. B. Mann, J. Chem. Phys., 47 (1967) 1893.
26 A H. Narten and H. A. Levy, "Water: A Comprehensive Treatise." Edited by F. Franks, Vol. I, p. 314. Plenum, New York 1972.
27 B. E. Warren and R. L. Mozzi, Acta Crystallogr., 21 (1966) 459.
28 A. H. Narten, J. Chem. Phys., 70 (1979) 299.
29 ^{13}C NMR Spectra Collection Sadtler Research Lab. (1984) (1981).
30 Data on X-ray powder patterns on TAAX, to be published, see also other references on TAAX, above [7, 8, 11, 13, 14, 20].

31 F. A. Bovey, "Chain Structure and Conformation of Macromolecule." Academic Press, New York, NY 1982.
32 A. E. Tonelli, "NMR Spectroscopy and Polymer Microstructure: The Conformational Connection." VCH Publishers, Inc., New York 1989.
33 P. J. Flory, "Statistical Mechanics of Chain Molecules," Wiley-Interscience, New York 1969.
34 T. Yoshida, K. Nagata, M. Yasuniwa, M. Yoshimatsu and B. Wunderlich, Acta Cryst., C50, 1758 (1994), see also Ref. [20).
35 J. R. Lyerla, Jr. and G.C. Levy, "Topics of Carbon-13 NMR Spectroscopy," Vol.1, John Wiley & Sons, New York 1974.
36 B. Wunderlich, "Macromolecular Physics, Vol. 1, Crystal Structure, Morphology, Defects." Academic Press, New York, NY 1973.
37 B. Wunderlich, M. Möller, J. Grebowicz and H. Baur, "Conformational Motion and Disorder in Low and High Molecular Mass Crystals." Springer Verlag, Berlin, 1988, (Adv. Polymer Sci., Vol. 87).